Journal of
Water & Climate Change

IWA PUBLISHING

Journal of Water and Climate Change Vol 15 No 2, 652 doi: 10.2166/wcc.2023.526

Analysis of the effect of rainfall center location on the flash flood process at the small basin scale

Guangzhao Chen [a], Jingming Hou [a,*], Tian Wang[a], Xujun Gao[b], Dangfeng Yang[b] and Tao Li[c]

[a] State Key Laboratory of Eco-hydraulics in Northwest Arid Region, Xi'an University of Technology, Xi' an, Shaanxi 710048, China
[b] PowerChina Northwest Engineering Corporation Limited, Xi'an 710065, China
[c] Yellow River Institute of Hydraulic Research, YRCC, Zhengzhou 450003, China
*Corresponding author. E-mail: jingming.hou@xaut.edu.cn

ABSTRACT

With the increasing frequency of extreme convective weather, the spatial–temporal variability of rainfall becomes more diversified. As a result of the insufficient quality of rainfall monitoring data in mountainous areas, the flash flood simulation usually does not consider the effect of the rainfall center location. In this work, the GPU Accelerated Surface Water Flow and Associated Transport hydrodynamic model is used to simulate the flash flood discharge process. The effect of the rainfall center location and the basin scale on the discharge process were analyzed based on simulated data. The results show that when the rainfall center is in the upstream and midstream basins, because of gravitational potential energy conversion, the total flood volume and the flood peak discharge increase to 2–10 times, and the peak time of flash flood caused by 100 mm rainfall amount can be advanced by up to 3,000 s compared to the 20 mm rainfall amount condition. The peak discharge and the delay of peak time increase with the increase of rain peak coefficient. In addition, the increase of the basin area enhances the effect of the rainfall center location. This work is helpful to quantify the effect of the rainfall center location, which can clarify the uncertainty of flash flood simulation caused by not considering the rainfall center factor.

Key words: Chicago rainfall pattern, flash flood, hydrodynamic model, rainfall center location, small basin

HIGHLIGHTS

- When the rainfall center is in the upstream and midstream basins, the total flood volume and the peak discharge increase to about 2–10 times, the flood peak time can be advanced by 3,000 s.
- The flood peak discharge increases with the increase of the rain peak coefficient, while the delay of the flood peak time is longer.
- The increase of the basin area enhances the effect of the rainfall center location on flash flood.

GRAPHICAL ABSTRACT

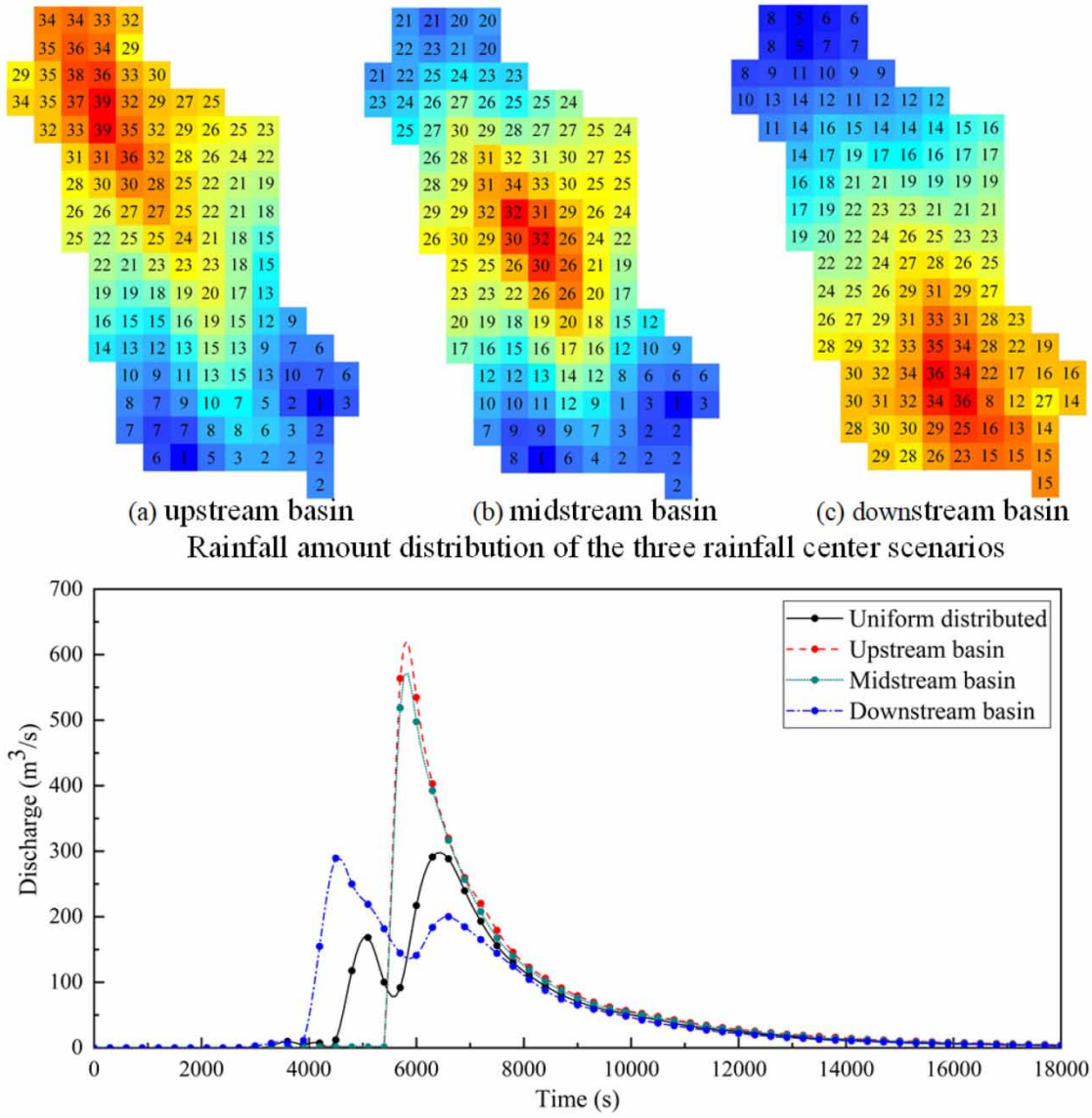

1. INTRODUCTION

Flash flood is caused by heavy rainfall in the mountainous area, which is characterized by its suddenness, wide-ranging danger, and difficulty in prediction (Ahmadalipour & Moradkhani 2019). In Europe, 40% of flood-related deaths between 1950 and 2006 were attributed to flash flood (Barredo 2007). In the United States, flash flood is the deadliest type of flood event (Alipour *et al.* 2020). Furthermore, 82% of the casualties from flood disasters in China between 2010 and 2016 were caused by flash flood (Liu *et al.* 2018b). Unfortunately, with an increase in the heavy precipitation event, future flash flood incidents may become more frequent (Alipour *et al.* 2020). Under the influence of global climate change, the uneven temporal–spatial distribution of extreme rainfall events is on the rise, which will seriously affect flash flood processes (Chen *et al.* 2020). As the temporal–spatial variability of rainfall becomes more complex, the accuracy of flash flood simulation methods that do not consider the rainfall center location will be compromised.

The temporal–spatial structure of rainfall has a significant impact on the hydrological response of flood (Zhu *et al.* 2018). In recent years, many researchers have studied the temporal–spatial characteristics of rainfall and their influence on flash flood. Llasat *et al.* (2014) analyzed flash floods in the northwest Mediterranean and concluded that flash flood is triggered by

intense, short-duration, and localized rainfall with convective characteristics. Emmanuel *et al.* (2015) developed rainfall spatial variability indices to detect the influence of rainfall spatial variability on the hydrological response. Silvestro *et al.* (2016) studied the impact of rainfall spatial distribution on flood discharge. Wright *et al.* (2020) developed a method for flood frequency analysis, considering rainfall variability. The impact of rainfall on flash flood is complex and related to the basin area, and it may be influenced by other terrain factors such as soil moisture and slope (Crow *et al.* 2017; Rogger *et al.* 2017). Zhou *et al.* (2021) found that the spatial heterogeneity of land use complicates the transformation of rainfall into flood. Grillakis *et al.* (2016) demonstrated that accurate soil moisture estimation can improve flood simulations. Besides, the relative importance of rainfall temporal and spatial characteristics is also a crucial research focus. Yang *et al.* (2016) found that in flood simulations, the temporal resolution of rainfall data is more important than spatial resolution. It is worth noting that most of the conclusions regarding the impact of rainfall temporal–spatial heterogeneity on flash flood is based on a relatively limited basin and rainfall event data. Limited monitoring data cannot provide detailed information about how the spatial–temporal distribution characteristics of rainfall affect flash flood. Flash flood results from complex interactions between spatiotemporal heterogeneity rainfall events, non-uniform surface features, and river network distribution, making conclusions drawn from specific basins and rainfall events somewhat specific (Zhu *et al.* 2018). In a basin, due to significant variations in morphological parameters across different regions, such as river width and length, bifurcation ratio, river density, elevation changes, basin perimeter, and area, the contribution of each local area to triggering floods differs (Oborie & Rowland 2023). This creates the need for more morphometric statistical analysis to understand the relationship between rainfall and flash flood under complex basin conditions. Furthermore, the relationship between rainfall and floods is basin scale-dependent (Zhou *et al.* 2021). However, there has been relatively little research focused on a small basin scale, and the impact of basin size on flash flood processes with different rainfall center locations still requires further investigation (Peleg *et al.* 2017).

High-quality rainfall information is crucial for the accurate simulation of flood (Wright *et al.* 2014). Measuring rainfall at individual locations using rain gauges is straightforward and has been widely used by researchers for decades, significantly advancing the study of rainfall-induced flood. However, as flood results from the combination of extreme rainfall events across a basin rather than at single points, the limitation of rain gauge has become increasingly apparent as flood modeling efforts progress (Wright 2018). The establishment of the dense rain gauge network can effectively monitor the temporal–spatial characteristics of rainfall. Nevertheless, the complex terrain of the mountainous basin makes it challenging to provide a reasonable and comprehensive rain gauge coverage. Additionally, the installation of advanced weather radars comes with high costs, making it unaffordable for many regions (Novák *et al.* 2021). With the advancement of satellite remote sensing technology, new methods have been introduced for rainfall prediction, showing excellent performance in large-scale and long-term rainfall prediction. However, the prediction accuracy for sudden rainfall events in local mountainous areas is relatively low (Wang & Wang 2022; Gultepe 2023). This underscores the need for a deeper understanding of the mechanisms through which rainfall temporal–spatial heterogeneity affects flash flood and for incorporating these effects fully into models to improve flash flood prediction (Saharia *et al.* 2021). Today, due to the efficiency and capabilities of Artificial Intelligence (AI) technology, various AI computational algorithms such as artificial neural networks, binary logistic regression, and entropy weights method have been widely applied to address water-related issues (Samadi *et al.* 2021; Borjalilu & Bozorgi-Amiri 2022; Dinh *et al.* 2022). Fayaz *et al.* (2022) proposed that a rainfall prediction algorithm based on the adaptive linear M5 model tree was proposed and demonstrated good predictive performance in the study area. However, these AI algorithms employ 'black-box' methods to provide results, where users can only analyze input and output values without understanding the internal workings of the algorithms, leading to decreased reliability and confidence in prediction. Additionally, issues such as low generalization ability, local minima, and overfitting may affect the stability of AI algorithms (Samadi *et al.* 2020). Currently, numerous hydrological models are applied in the numerical simulation of flash flood, such as the Hydrologic Engineering Center's-Hydrologic Modeling System (HEC-HMS) and the Variable Infiltration Capacity (VIC) model. These hydrological models offer high computational efficiency and are fairly accurate in simulating flood processes (Hu & Song 2018). However, the high-computational efficiency of the hydrological model is achieved by simplifying hydrological processes and setting numerous conceptual parameters, resulting in less than perfect simulation performance. It is necessary to use a more accurate model for simulation, and the hydrodynamic model coupled with hydrological processes, which simulate the flood progression process based on the laws of fluid dynamics, can address this issue. With rapid advancements in computer technology, the computational burden no longer hampers the widespread application of the hydrodynamic model (Ming *et al.* 2020). It can effectively capture the influence of micro-topography on runoff.

Therefore, the lack of sufficient high-resolution rainfall data and the hydrodynamic model that has high-computational efficiency and accuracy poses the greatest obstacles to constructing the simulation model that investigate the impact of spatiotemporal changes in heavy rainfall on flash flood. This study utilizes the Graphics Processing Unit (GPU) Accelerated Surface Water Flow and Associated Transport (GAST) hydrodynamic model, which employs GPU acceleration technology and is based on solving the shallow water equations to simulate high-precision flash flood processes. And by constructing high-resolution rainfall data with different characteristics, the study analyzes the impact of the rainfall center location on flash flood processes in the small basin. Furthermore, the study examines variations in flash flood processes resulting from the combined effects of the basin scale and the rainfall center location.

2. METHODOLOGY

2.1. The GAST model

The GAST model is coupled with hydrological and hydrodynamic processes (Hou *et al.* 2021). The governing equation is the shallow water equation, which can be written as:

$$\frac{\partial q}{\partial t}+\frac{\partial f}{\partial x}+\frac{\partial g}{\partial y}=S \tag{1}$$

$$q=\begin{bmatrix} h \\ q_x \\ q_y \end{bmatrix},\quad f=\begin{bmatrix} uh \\ uq_x+gh^2/2 \\ uq_y \end{bmatrix},\ g=\begin{bmatrix} vh \\ vq_x \\ vq_y+gh^2/2 \end{bmatrix}$$

$$S=\begin{bmatrix} i \\ -\dfrac{gh\partial z_b}{\partial x}-C_f u\sqrt{u^2+v^2} \\ -\dfrac{gh\partial z_b}{\partial y}-C_f v\sqrt{u^2+v^2} \end{bmatrix} \tag{2}$$

where t denotes the time; x and y represent the Cartesian coordinates; $\boldsymbol{q}$ is the vector of flow variables containing the water depth h, in which q_x and q_y are the discharges in the x- and y- directions, respectively; u and v are depth-averaged velocities in the x- and y-directions, respectively; z_b denotes the bed elevation; $\boldsymbol{f}$ and $\boldsymbol{g}$ are the flux vectors in the x- and y-directions, respectively; $\boldsymbol{S}$ represents the source vector; C_f is the bed roughness coefficient.

Apart from the Manning coefficient, the infiltration rate is another parameter that influences the simulation results. The Green–Ampt (G–A) algorithm is used to describe the soil infiltration characteristics (Hou *et al.* 2021). It is assumed that the inundation depth on the soil surface is negligible compared with the soil depth, and the control equation of the G–A algorithm is Equation (3). The soil infiltration rate i_r in the study area is calculated by Equation (3). The f_p is directly used to calculate the source vector i in Equation (2), which is equal to i_r–f_p, where i_r is the rainfall rate. When $i_r \le K_s$, the accumulated infiltration F is calculated at each time step dt, and the infiltration value f_p is equal to i_r. In addition, it is necessary to check whether the accumulated infiltration F exceeds the cumulative infiltration capacity F_s. The equation of F_s is Equation (4). The equation of the cumulative infiltration rate for each time step is Equation (5)

$$f_p=\begin{cases} i_r & i_r \le K_s \\ K_S[1+(\theta_S-\theta_i)S_f/F] & i_r > K_s \end{cases} \tag{3}$$

$$F_s=\frac{K_S S_f(\theta_s-\theta_i)}{i-K_S} \tag{4}$$

$$F_{n+1}=K_S+S_f(\theta_s-\theta_i)\ln\left(1+\frac{F_n}{S_f(\theta_s-\theta_i)}\right) \tag{5}$$

where K_S is the soil saturated hydraulic conductivity (mm/min); θ_i is the initial soil water content; θ_S is the saturated soil water content; S_f is the wetting front suction (mm); i_r is the rainfall intensity (mm/min); t is the simulated time; t_p is the time when runoff begins to appear; F is the accumulated infiltration (mm).

The G–A algorithm adopts different calculated parameters according to the land use information on the calculated cell when calculating the infiltration rate in each calculated cell, so as to simulate the infiltration rate of different land uses.

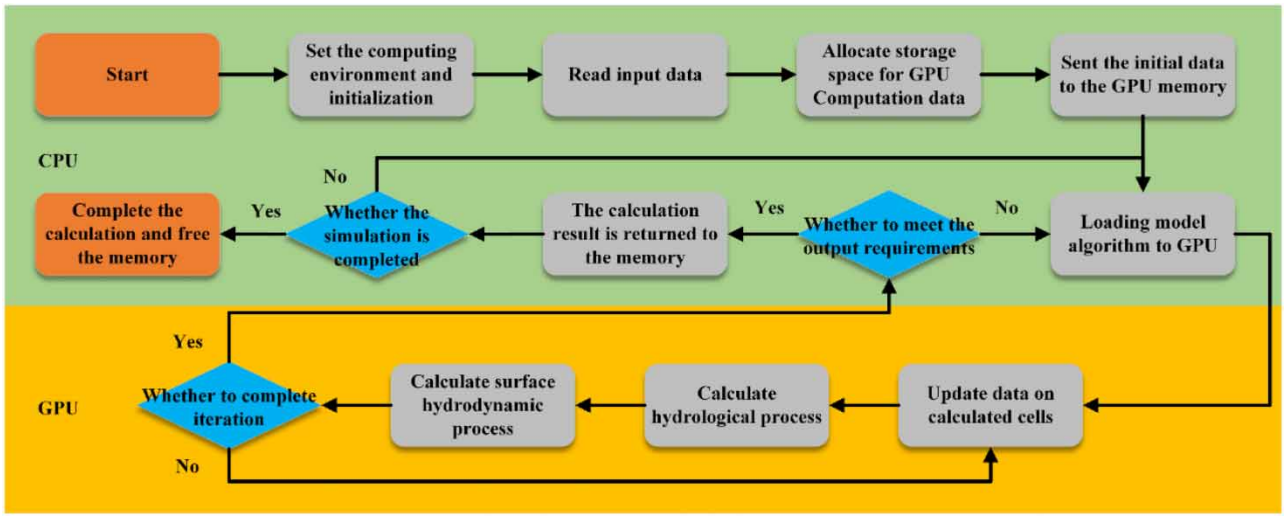

Figure 1 | Workflow of the GAST model.

Due to the lack of data on trees in the study area, the canopy effects and interception are not calculated separately. Some of the rainfall intercepted by it is considered to be lost through soil infiltration. Infiltration parameters will be determined through model validation Workflow of the GAST model is shown in Figure 1.

2.2. Evaluation indicator

The formula of the Nash–Sutcliffe efficiency (NSE) coefficient is Equation (6). (If NSE is on the brink of 1, it means the simulated result is reliable).

$$\mathrm{NSE} = 1 - \frac{\sum_{i=1}^{N} \left(q_i^{\mathrm{obs}} - q_i^{\mathrm{sim}}\right)^2}{\sum_{i=1}^{N} \left(q_i^{\mathrm{obs}} - q_i^{-\mathrm{obs}}\right)^2} \tag{6}$$

where q_i^{sim} is the simulated data sequence; q_i^{obs} is the observed data sequence; $q_i^{-\mathrm{obs}}$ is the average value of the observed data; N is the number of the observed data.

The root-mean-square error (RMSE) is another common index for assessing model performance. RMSE = 0 means that the simulated data match the measured data exactly; if the RMSE is less than half of the standard deviation (σ) of the measured data, the model has good performance. The formula is as follows:

$$\mathrm{RMSE} = \sqrt{\frac{\sum_{i=1}^{n} \left(Q_{\mathrm{m}}^i - Q_{\mathrm{s}}^i\right)^2}{n}} \tag{7}$$

where Q_{m}^i is the measured data at time i; Q_{s}^i is the simulated data at time i; n is the amount of data.

The R^2 is used to evaluate the similarity between the simulated values from the numerical model and the observed values. The closer the value is to 1, the better the numerical model performance is. The formula is as follows:

$$\mathrm{MAPE} = \frac{1}{n} \sum_{i=1}^{n} \left| \frac{Q_{\mathrm{m}}^i - Q_{\mathrm{s}}^i}{Q_{\mathrm{m}}^i} \right| \tag{8}$$

where the meaning of parameters is the same as that in Equation (5).

Drawing on the concept of the NSE coefficient, this work proposes the deviation index E to quantitatively evaluate the magnitude of the difference between the flash flood process with non-uniform rainfall spatial distribution and that with

uniform rainfall spatial distribution. The calculation formula is shown in Equation (9), where the index closer to 1 means that the difference is smaller and *vice versa* represents it has a larger difference.

$$E = 1 - \frac{\sum_{i=1}^{N} \left(p_i^{\text{non-uniform}} - p_i^{\text{uniform}}\right)^2}{\sum_{i=1}^{N} \left(p_i^{\text{non-uniform}} - p_i^{-\text{uniform}}\right)^2} \tag{9}$$

where $p_i^{\text{non-uniform}}$ is the flood data with non-uniform rainfall space distribution; p_i^{uniform} is the flood data with uniform rainfall space distribution; $p_i^{-\text{uniform}}$ is the average value of the flood data with uniform rainfall space distribution; N is the amount of data.

3. EXPERIMENTAL DESIGN

3.1. Basin data

The Baogaisi basin is located in Hunan Province, China, with a total area of about 56 km^2. The longitude and latitude of the basin center are 113 °43′56″E, 28 °21′50″N. The location is shown in Figure 2(a). The land use of the hillside and the river channel are forest land and bare soil, respectively. The average slope of the river channel is 4%, and the hillside slope is 4.5%. The topography of the Baogaisi basin has typical V-shaped geomorphic characteristics of the small-scale basin, and there is no unique landform. Therefore, using this basin to study the effect of the variation of the rainfall center location on the flash flood process at the small basin scale can avoid the particularity of the conclusion. The Digital Elevation Model (DEM) data were obtained from the local mapping bureau with a resolution of 10 m. The DEM data and the land use map are shown in Figure 2.

The V-shaped basin is a simplification of the actual basin and can represent the actual basin shape. It provides a convenient way to study the change of flash flood under different terrain conditions. This work is based on the concept of the V-shaped basin to construct the terrains with different areas and study the change of discharge under the same rainfall characteristics. In Figure 3, S1 and S2 represent the slope of the hillside and the slope of the river channel, respectively; L_C and L_O are the basin length and the width of hillside, respectively; W and D are the width and depth of the river channel at the basin entrance, respectively. The Manning coefficient comes from the literature (Simons *et al.* 2014). Therefore, the Manning coefficient of the hillside is 0.015, and the Manning coefficient of the river channel is 0.15.

Topographic features of the V-shaped basin can be altered by changing parameters, such as slope and area. Three V-shaped basins were used in this work to investigate the effect of the basin area on the study results. The parameters of each V-shaped basin are shown in Table 1. V1 is the prototype of the V-shaped basin. The area size of V2 is larger than V1, and the area size of V3 is larger than V2. These three terrains were used in this work to investigate the impacts of the area size of the basin on the flash flood process.

3.2. Rainfall data

In this work, the generation of rainfall data is realized from the aspects of rainfall spatial distribution and rainfall temporal distribution. The first step is to design the spatial distribution of rainfall. According to the reference (Ochoa-Rodriguez *et al.* 2015), the spatial resolution of rainfall cell is set to 500 m. Therefore, the entire basin is divided into 234 rainfall grids. Along the direction of the river channel, the entire basin is evenly divided into three parts: upstream, midstream, and downstream. Three rainfall center locations were designed. They are also located upstream, midstream, and downstream, respectively. The rainfall amount of each rainfall cell was obtained by Kriging interpolation in the ArcGIS software. In the ArcGIS, the control points are set up uniformly every 1 km along the northwest – southeast direction of the river channel. In each rainstorm scenario, the rainfall amount at the control point where the rainstorm center is located is the maximum; the rainfall amount at other control points gradually decreases as the distance from the control point at the rainstorm center increases. Figure 4 shows the rainfall amount distribution of three rainfall center scenarios with 20 mm accumulative rainfall amount. In Figure 4, the values in each rainfall grid represent the rainfall amount.

The second step is to design the temporal distribution of rainfall. The Chicago rainfall pattern can be used to describe the short-duration rainfall process in the study area, which is usually generated rainfall data with 2 h duration (Li *et al.* 2018). Ochoa-Rodriguez *et al.* (2015) identified that the optimal temporal resolution applicable to the simulation is 5 min. Therefore, the rainstorm temporal resolution is 5 min, and the duration is 2 h in this work.

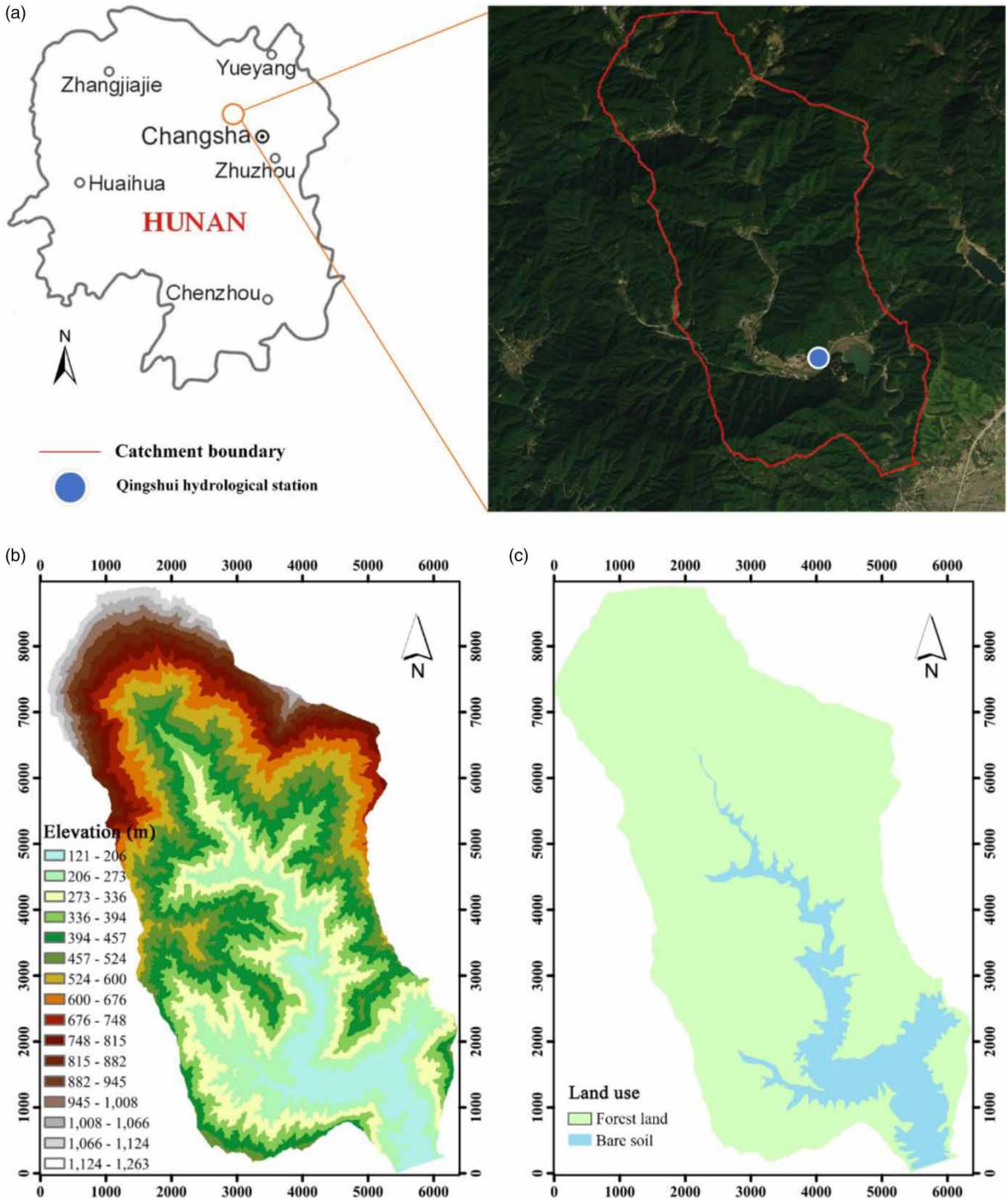

Figure 2 | Location and terrain data of the basin: (a) location; (b) DEM; and (c) land use.

Flash floods are associated with intense rainfall in a short duration and affecting small areas (Gaume *et al.* 2009). The Chicago rainfall pattern is a design rainfall pattern with short duration based on multi-year rainfall data. This work mainly focuses on flash flood events caused by short-duration intense rainfall at the small basin scale. Therefore, the Chicago rain pattern is selected to construct the rainfall data. The Chicago rainfall equations (Equations (10)–(12)) are used to generate the rainfall process. Three rain peaks (rain peak coefficient $r = 0.2$, 0.5, and 0.8) are designed. The percentage distribution

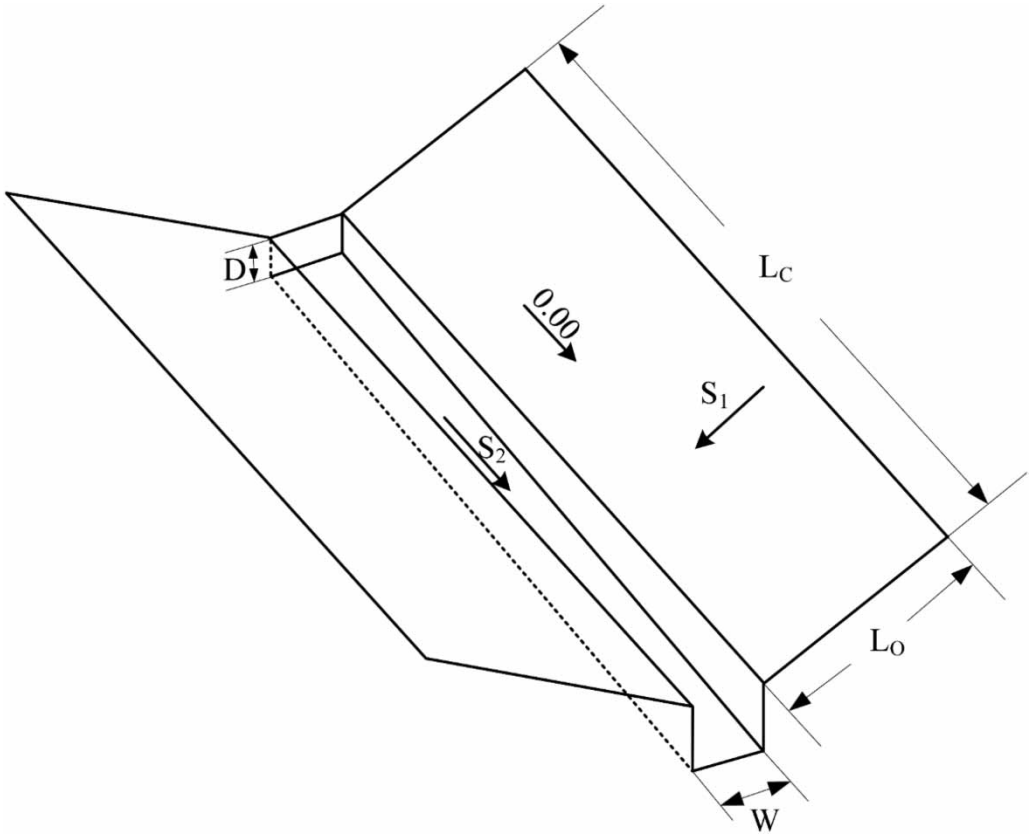

Figure 3 | V-shaped basin structure.

Table 1 | The parameters of different V-shaped ideal basins

	S_1	S_2	L_C (m)	L_O (m)	W (m)	D (m)
V1	0.01	0.01	1,000	800	20	20
V2	0.01	0.01	5,000	4,000	100	100
V3	0.01	0.01	10,000	8,000	200	200

of rainfall amount derived from the Chicago rain pattern is shown in Figure 5. Besides, five rainfall amounts (20, 40, 60, 80, and 100 mm) are selected for further analysis.

$$i = \frac{A(1 + C\lg P)}{(t+b)^n} = \frac{6.838(1 + 0.54\lg P)}{(t+8.277)^{0.5127}} \tag{10}$$

$$i_a = \frac{a\left[\frac{(1-n)t_a}{r} + b\right]}{\left(\frac{t_a}{r} + b\right)^{1+c}} \tag{11}$$

$$i_b = \frac{a\left[\frac{(1-n)t_b}{1-r} + b\right]}{\left(\frac{t_b}{1-r} + b\right)^{1+c}} \tag{12}$$

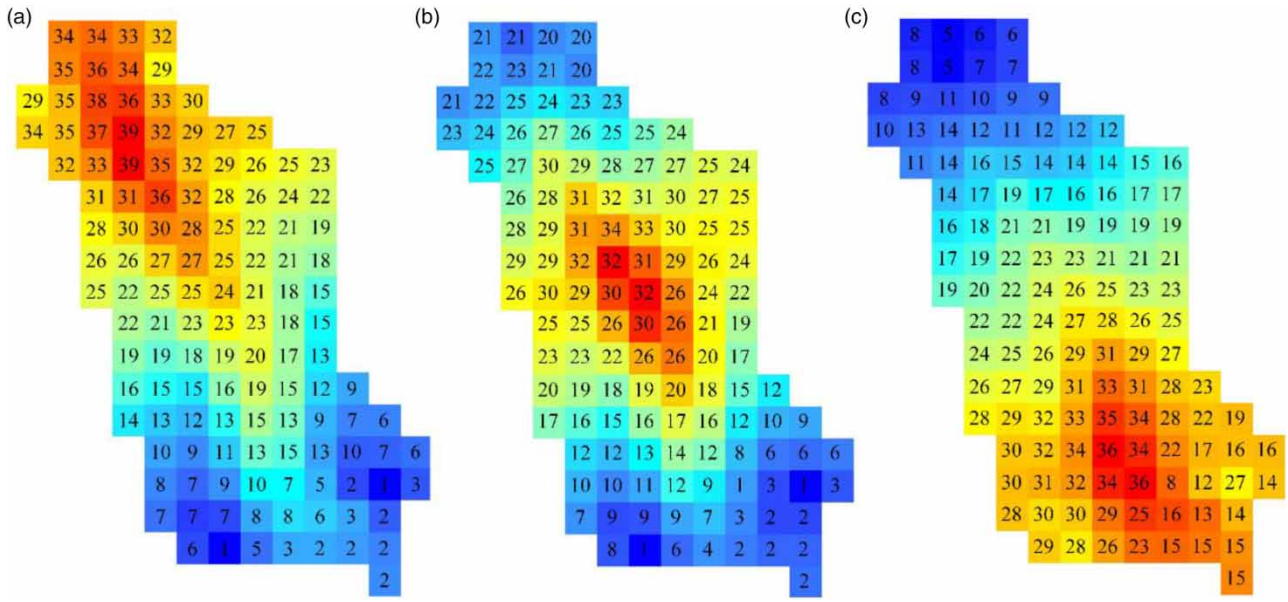

Figure 4 | Rainfall amount distribution of the three rainfall center scenarios: (a) upstream basin; (b) midstream basin; and (c) downstream basin.

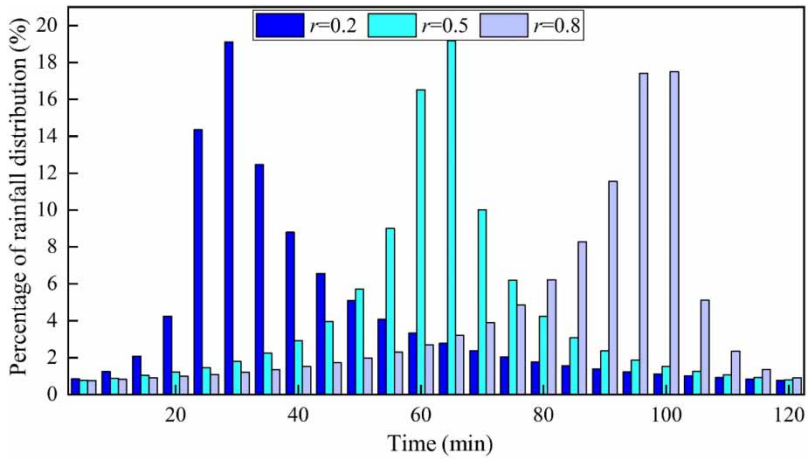

Figure 5 | Percentage distribution of the three rain peaks.

where i is the rainstorm intensity (mm/min), P represents the return period (a), t is the rainstorm duration (min), n is the rainstorm attenuation index, b and C are the constants, and A is the rainfall with a return period of 1 year (mm).

There are four types of rainfall center locations (including uniform-distributed rainfall), three types of rain peak coefficients, and five types of rainfall amount. The total number of simulated cases is $4 \times 3 \times 5 = 60$. The simulated scenarios are shown in Table 2.

4. RESULTS AND DISCUSSION

4.1. Model validation

The rainfall data and water level data used for model validation were obtained from the Qingshui hydrological station. The rainfall data for model validation is from May 9, 2012 and June 6, 2013. According to the government's 2021 Soil Moisture Briefing in Liuyang City, Hunan Province, the soil type in the Baogaisi basin is red loam. However, since the soil texture

Table 2 | Rainfall simulated scenarios with different rainfall center locations and other rainfall factors

Scenario number	Accumulative rainfall	Rain peak coefficient	Rainfall center location
1	20	$r = 0.2$	Upstream basin
2	20	$r = 0.2$	Midstream basin
3	20	$r = 0.2$	Downstream basin
...	...	...	...
11	20	$r = 0.5$	Uniform distributed
12	20	$r = 0.8$	Uniform distributed
...	...	...	...
24	40	$r = 0.8$	Uniform distributed
...	...	...	...
60	100	$r = 0.8$	Uniform distributed

varies from place to place, the values of each soil parameter were determined by considering the parameter values already used in the reference study conducted in this area for research (Liu *et al.* 2018a). The soil-saturated hydraulic values in the river channel and the hillside are 0.333 and 0.100 mm/min, respectively. The river of the Baogaisi basin is an intermittent river. When no rainfall occurs, the river is usually water-free and the soil at the river bottom is exposed, so the soil infiltration of the river channel needs to be considered. The wetting front suctions are 50 and 20 mm, respectively. The Manning coefficients are 0.02 and 0.2, respectively.

It can be seen from Figure 6 that the simulated water level data and the observed data have a high agreement. The NSE, RMSE, and R^2 of the data in Figure 6(a) are 0.95, 0.048, and 0.98, respectively. The RMSE of the data in Figure 6(a) is less than half of the standard deviation (0.105). Meanwhile, the NSE, RMSE, and R^2 of the data in Figure 6(b) are 0.92, 0.051, and 0.00024, respectively. The RMSE of the data in Figure 6(b) is also less than half of the standard deviation (0.105). It shows that this model can accurately simulate the flash flood of the Baogaisi basin.

Detailed information on the GAST model validation for the V-shaped basin has been presented in the literature (Hou *et al.* 2018). The NSE of simulated runoff data and analytical solution for the hillside is 0.99 and for the river channel is 0.98. This shows that the simulation of this model is accurate and can reproduce the runoff process of the V-shaped basin well. In this work, the same GAST model was used to simulate the flash flood discharge process in terrain V1, terrain V2, and terrain V3.

4.2. Influence of the rainfall center location on the flash flood process

Taking the rainfall amount of 40 mm and the rain peak coefficient $r = 0.5$ as an example, the effect of the rainfall center location on the flood process is illustrated. The flood discharge processes at the basin outlet with different rainfall center locations are shown in Figure 7. Because of the complex micro-topography of the Baogaisi basin, the runoff generated at

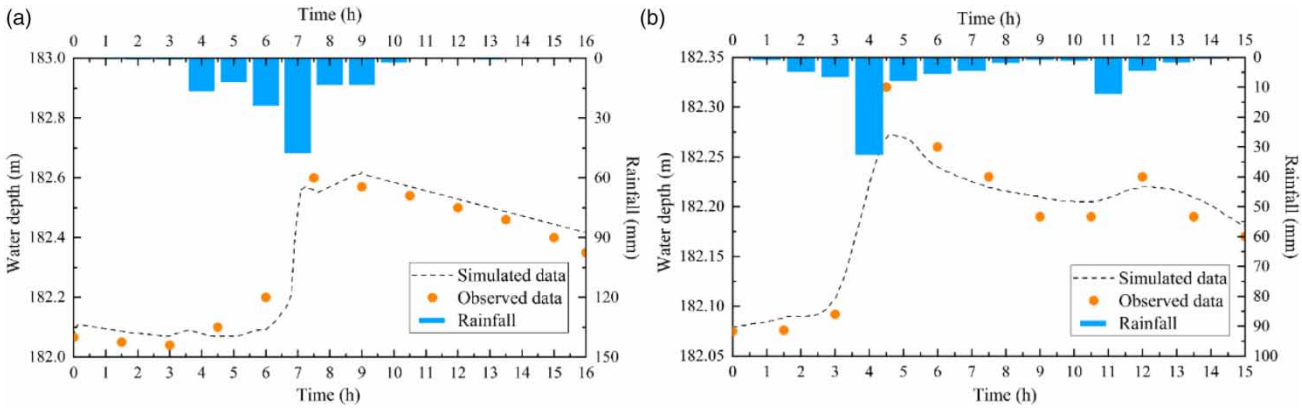

Figure 6 | Comparison of observed and simulated data.

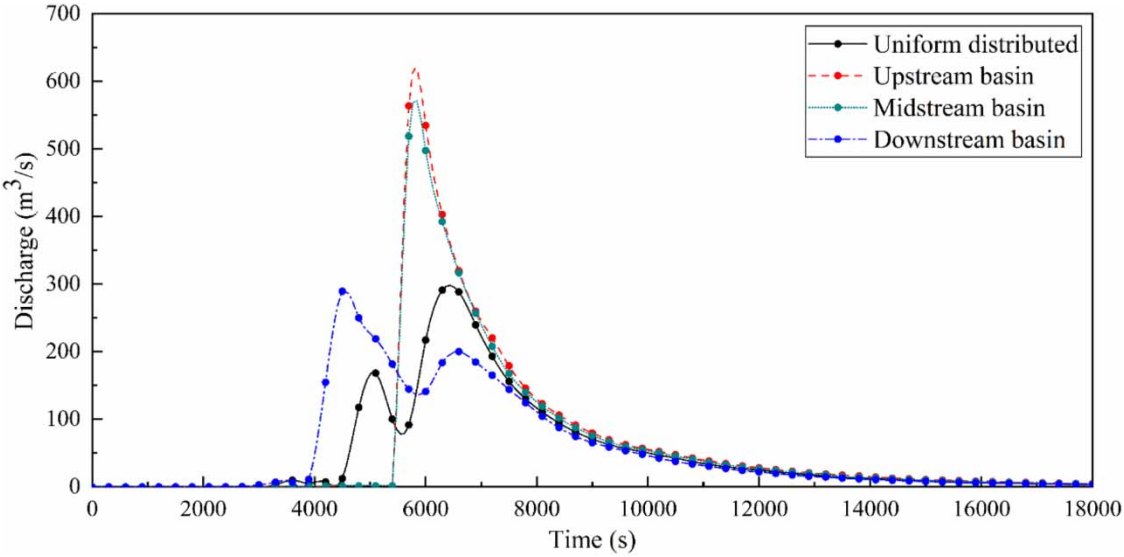

Figure 7 | Flood discharge process of the outlet under different rainfall spatial distributions.

different locations flows to the river channel at long intervals. In this situation, a single flood peak cannot be formed at the basin outlet. On the contrary, the discharge process has multiple small flood peaks. This phenomenon is like the phenomenon at the reference (Huang *et al.* 2018). Therefore, the flood process under the condition of uniform rainfall spatial distribution in Figure 7 is bimodal. In this study, three distinct rainfall center locations were designed: the upstream basin, the midstream basin, and the downstream basin. When the rainfall center is in the upstream and midstream basins, the rainfall is mainly concentrated in the mountainous regions with a steep slope. The runoff has a large gravitational potential energy at higher elevations, and its own gravitational potential energy will be converted into kinetic energy when flowing to the basin outlet (Zwawi & Algarni 2019). It speeds up flow velocity, so that the runoff from the upstream and midstream basins can merge with the runoff from the downstream basin at the basin outlet. This is consistent with Marchi *et al.* (2010), which shows that steep slopes are a prominent morphological feature in flash flood-prone basins, promoting rapid runoff concentration and increasing the likelihood of flash flood occurrences. In this situation, the flood process eventually becomes a single-peaked pattern. When the rainfall center is in the downstream basin, there is no acceleration effect of flow velocity from gravitational potential energy. Therefore, the flow process still has a double-peaked pattern when the rainfall center is in the downstream basin.

The discharge processes at the basin outlet with different rainfall amounts are shown in Figure 8. In the case of non-uniform rainfall spatial distribution, the flood process becomes sharper as the rainfall amounts increase, and the flood peak time is earlier. This is consistent with the change law of the flood process in the uniform rainfall case with the increase of the rainfall amount. It is noteworthy that the variation of the flash flood process differs when the rainfall center is in the downstream basin. At the small rainfall amount, the discharge process remains as a double-peaked characteristic during uniform rainfall condition. As the rainfall amount increases, the first flood peak gradually becomes smaller to disappear completely and the discharge process changes to a single-peaked pattern.

Through the comparison of the discharge process shown in Figure 8, when the rainfall amount is 20 mm, the rainfall center location has the greatest influence on the outlet discharge process. When the rainfall amount reaches 100 mm, the rainfall center location has the least influence. It can be concluded that with the increase of rainfall amount, the effect of the rainfall center location on the flash flood process gradually decreases. The reduction of the flood peak time is the greatest when the rainfall center is in the downstream. However, the reduction of the flood peak time is similar both when the rainfall center is in the upstream and midstream basins and when it is smaller than when the rainfall center is in the downstream. In the simulated cases, both the total flood volume and the flood peak discharge increased by 2–10 times, and the flood peak time can be advanced by 0–3,000 s.

Wright *et al.* (2020) pointed out that the structure of heavy rainfall, including fine-scale variations and the rainfall temporal distribution, is a crucial factor influencing the flood processes. The effect of the rain peak coefficient on the discharge process

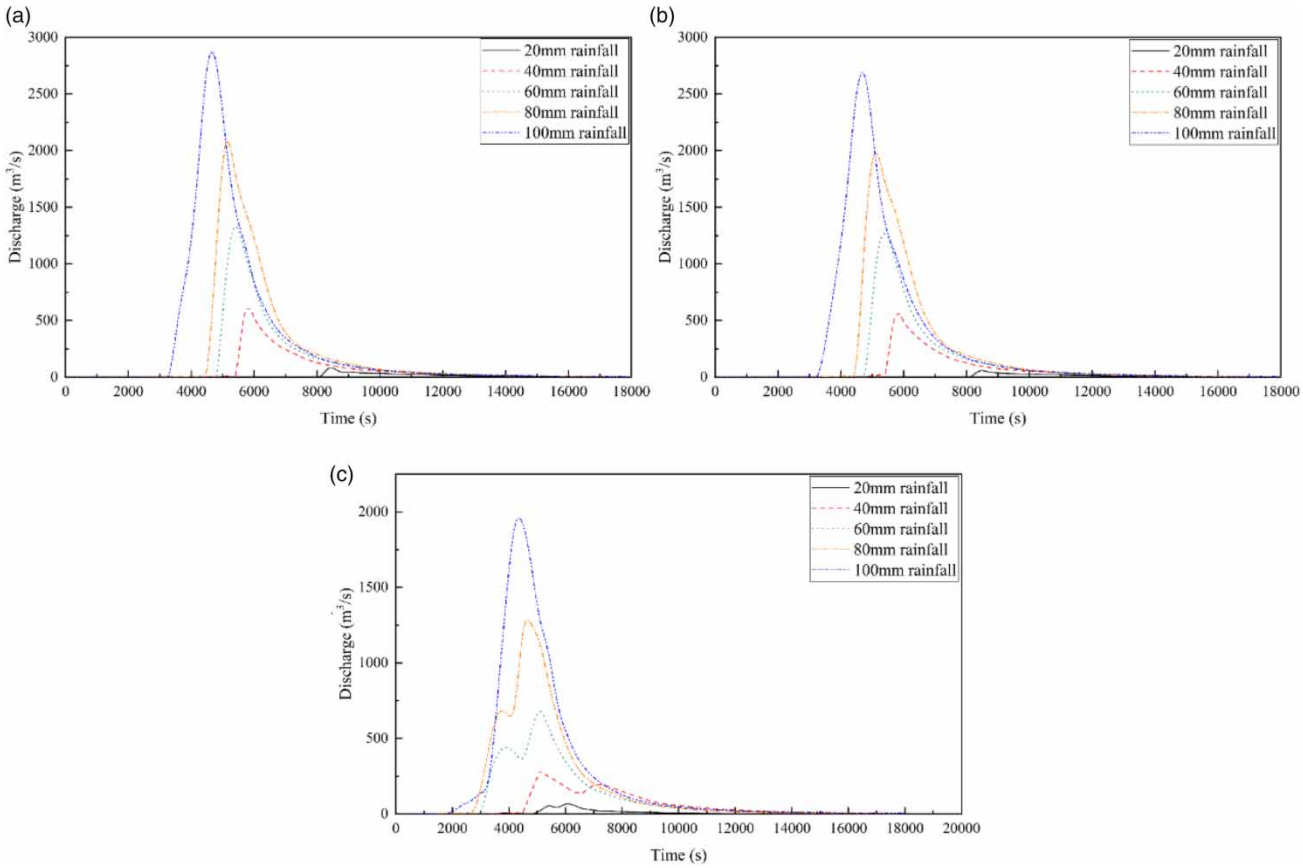

Figure 8 | Discharge process at the outlet with different rainfall amounts ($r = 0.5$): (a) rainfall center at the upstream; (b) rainfall center at the midstream; and (c) rainfall center at the downstream.

with different rainfall center locations is shown in Figure 9. The response of the discharge process to the rain peak coefficient for different rainfall center locations is consistent. The flood peak discharge increases with the increase of the rain peak coefficient, while the delay of the flood peak time becomes longer. Compared with the situation where rainfall is uniformly distributed, except when the rainfall center is in the downstream basin, the discharge process becomes sharper, the flood peak discharge increases and the flood peak time advances. When the rainfall center is in the downstream basin, at different rain peak coefficient conditions, the flood process does not become sharper, and the flood peak discharge decreases slightly, but the flood peak time is advanced. The deviation index E of the discharge process under different rain peak coefficients is shown in Table 3. From Table 3, we can observe that there is a direct relationship between the rain peak coefficient and the deviation of the discharge process when the rainfall is spatially non-uniformly distributed from that when rainfall is spatially uniformly distributed; the closer the rainfall center location is to the upstream basin, the greater the deviation of the discharge process when the rainfall is spatially non-uniformly distributed.

From the discharge processes as shown in Figure 9(a) and 9(b), when the rainfall center is in the upstream and midstream basins, the discharge processes differ little. But they are different from the flood processes shown in Figure 9(c), in which the rainfall center is in the downstream basin. A flow velocity map is shown in Figure 10. From the perspective of flow velocity, the cause may be related to the basin topography. In the flow velocity map, the direction of the arrow represents the flow direction. The longer the arrow, the faster the flow velocity. Taking the rainfall case with a rainfall amount of 40 mm and a rain peak coefficient $r = 0.5$ as an example, the flood peak discharge occurs at 5,700 s when the rainfall center is in the upstream and midstream basins; the flood peak discharge occurs at 4,500 s when the rainfall center is in the downstream basin. Meanwhile, the flood peak discharge occurs at 6,300 s when the rainfall is uniformly spatially distributed rainfall. When the rainfall center is in the downstream and midstream basins, the distance of runoff flow to the basin outlet is shortened; therefore, the flood peak time is significantly earlier. The closer the rainfall center is to the basin outlet, the more

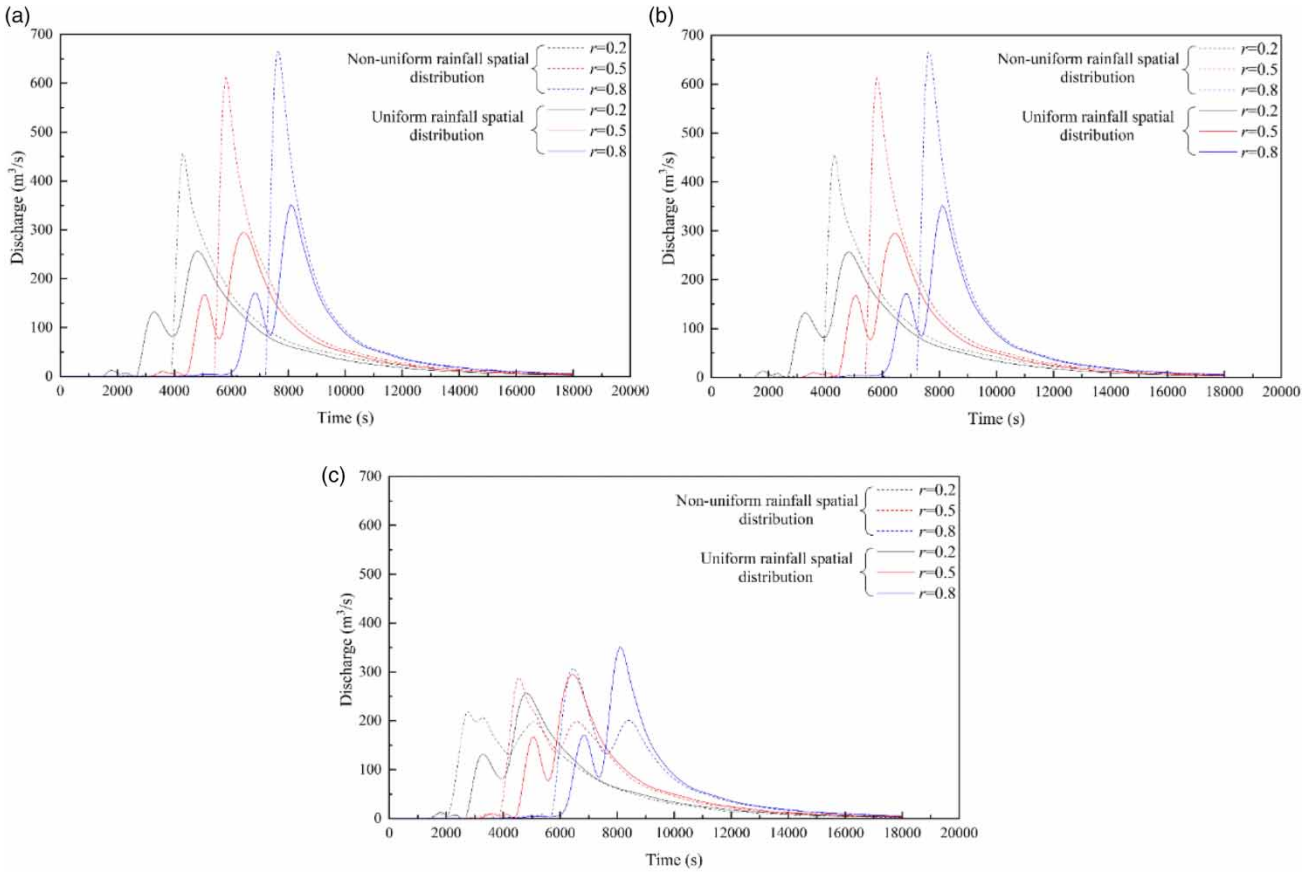

Figure 9 | Flash flood discharge process with different rain peak coefficients (40 mm): (a) rainfall center at the upstream; (b) rainfall center at the midstream; and (c) rainfall center at the downstream.

Table 3 | Deviation index *E* of the discharge process under different rain peak coefficients

Rain peak coefficient		0.2	0.5	0.8
The rainfall center location	Upstream basin	0.288	0.232	0.167
	Midstream basin	0.340	0.013	0.041
	Downstream basin	0.618	0.504	0.503

significantly the flood peak time is advanced (Borga *et al.* 2014, 2019; Braud *et al.* 2014). The flow velocity arrow in the river channel is very dense and long when the rainfall center is in the upstream and midstream basins, but the arrow is sporadic and short when the rainfall center is in the downstream basin. It shows that when the rainfall center is in the upstream and midstream basins, the runoff from the hillside quickly converges to the river channel, and the flow velocity is quick. The upstream terrain is the steepest in the entire basin, and it gives the runoff enormous gravitational potential energy. Therefore, when the rainfall center is in the upstream basin, although it increases the distance of flow to the outlet location, the stream-flow can maintain a high-flow velocity because of the conversion of gravitational potential energy into kinetic energy, which results in an earlier flood peak time. Therefore, when the rainfall center is located in the upper and middle reaches of the basin, the flood peak time is the same. Many scholars have studied the significant impact forces generated when high-altitude water flows downstream during the flash flood event through field experiments, flume tests, and numerical methods (Gu & Lei 2023). During flash flood, debris like tree branches and crop residues carried by the rushing water can block the river channel, forming a temporary 'water-blocking dam' (Hou *et al.* 2020). When these dams break, a 'cascade effect' occurs,

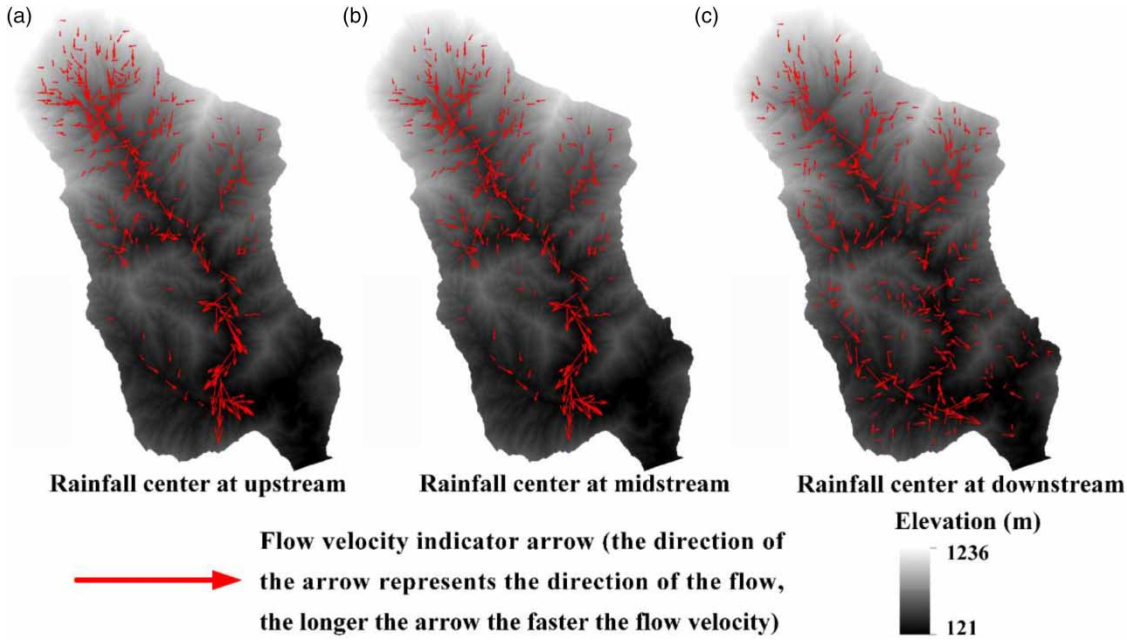

Figure 10 | Flow velocity map at the flood peak time (40 mm, $r = 0.5$). (a) Rainfall center at the upstream; (b) rainfall center at the midstream; and (c) rainfall center at the downstream.

where the energy of the high-level floodwater accumulates and is suddenly released with tremendous force, causing the water to rush downstream toward the outlet.

4.3. Impact of basin area size on the flash flood process with different rainfall center locations

Based on the V-shaped ideal basin, the influence of the basin area on flash flood with different rainfall center locations is investigated. The change of flood peak discharge under different rainfall center locations at different basin areas is shown in Figure 11. In V1, V2, and V3, the area of V1 is the smallest, V2 is twice that of V1, and V3 is twice that of V2. The influence degree of flood peak discharge is equal to the flood peak discharge caused by the non-uniform spatial distribution rainfall/the

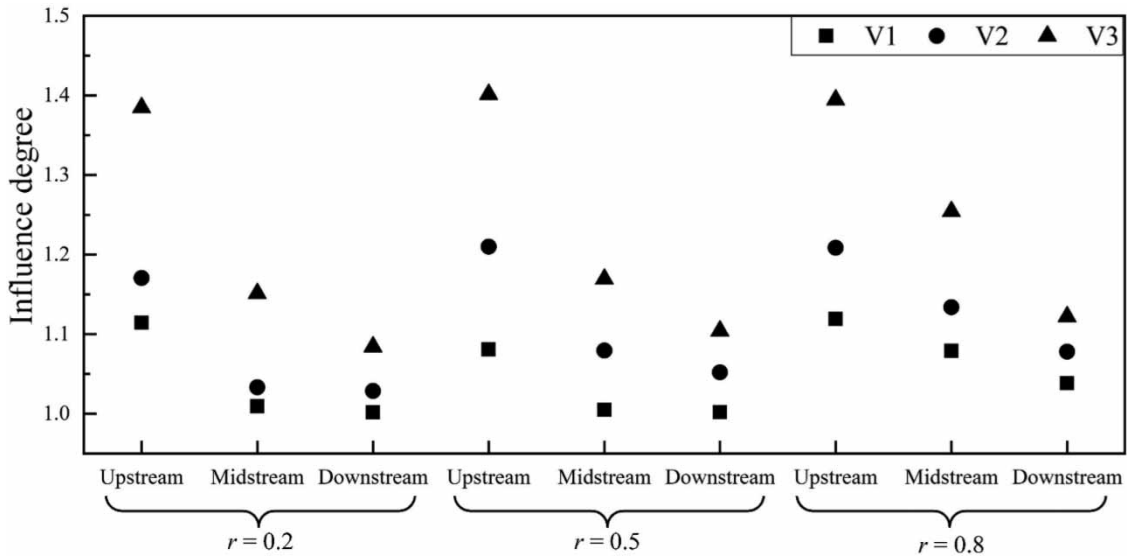

Figure 11 | The change of flood peak discharge under different rainfall center locations at different basin areas.

flood peak discharge of uniform caused by the spatial distribution rainfall. It can be seen from Figure 11 that the influence degree of flood peak discharge goes up with the expansion of the basin area. The increase of the influence degree varies with the rainfall center location and the rain peak coefficient, but the effect of the rain peak coefficient is small. When the rainfall center is in the upstream basin, the influence degree rises most significantly, followed by the midstream basin and the downstream basin.

In addition to the basin-scale parameters mentioned above, other morphological parameters also exert a significant influence on flood response (Oborie & Rowland 2023). Mountainous micro-topography is recognized as an important influential factor in the flash flood generation, because it affects flow-generating processes and streamflow situation (Borga *et al.* 2010). Therefore, in the ideal basin, the influence caused by the spatial and temporal variability of rainstorms can directly impact streamflow without being affected by micro-topography. In real-world basins, the simulation results are affected by the surface micro-topography, which is consistent with the findings of the existing research (Braud *et al.* 2014). The steep slopes in small catchments over complex mountainous terrains lead to rapid runoff yield and the concentration of moisture, with sudden and sharp rises and drops in water depth, which contribute to the rapid development of flash flood disasters (He *et al.* 2018). The influence of longitudinal and transverse slopes on flood processes under different rainfall conditions also needs to be further studied in the future. Longitudinal slope can directly affect the flood process within the river channel by altering the channel gradient, while transverse slope, by changing the slopes on either side of the hills, influences the runoff process indirectly and affects the flood processes at the basin outlet.

5. CONCLUSIONS

In this paper, the effect of the rainfall center location on the flash flood process at the small basin scale is investigated by using the GAST hydrodynamic model to simulate different flash flood processess under different rainfall center locations. Based on the results and discussion made, the following conclusions are drawn.

- When the rainfall center is in the upstream and midstream basins, the total flood volume and the flood peak discharge can increase up to 2–10 times due to gravitational potential energy conversion. The flood peak time can be advanced by up to 3,000 s. This uncertainty should be considered in flood warning systems, with appropriate deviation ranges for flood peak arrival time.
- As the rainfall peak coefficient increases, the flood peak discharge rises and the flood peak time delays. Emergency management should simulate different rainfall peak scenarios, considering different flood peak time for rational flood planning.
- The basin area amplifies the rainfall center's impact on flash flood. This effect is enhanced most significantly when the rainfall center is in the upstream basin, followed by the midstream and downstream basins. Therefore, emergency plans should account for the rainfall center location, lowering critical rainfall thresholds when it is in upstream.

This work quantitatively analyzes the variation in the flash flood discharge process with different rainfall center locations and clarifies its mechanisms. However, in this work, some characteristic information of rainfall was not considered, such as the spatial resolution of rainfall data (Lobligeois *et al.* 2014), different rainfall durations (Wei *et al.* 2019), and the temporal resolution of rainfall data (Wei *et al.* 2019). Changes in these factors may influence the conclusions drawn above, which requires further research.

ACKNOWLEDGEMENTS

This work is partly supported by the National Natural Science Foundation of China (Grant Nos. 52079106 and 52009104); the Sino-German Mobility Programme (Grant No. M-0427); Key Science and Technology Projects of Power China (DJ-ZDXM-2022-41); Major Company-Level Science and Technology Projects of Northwest Engineering Corporation Limited, Power China (XBY-ZDKJ-2022-9); Key R&D Program of Shannxi of China Key Technology and Industrialization of Sustainable Management of Flood Disaster (2023GXLH-042).

DATA AVAILABILITY STATEMENT

Data cannot be made publicly available; readers should contact the corresponding author for details.

CONFLICT OF INTEREST

The authors declare there is no conflict.

REFERENCES

Ahmadalipour, A. & Moradkhani, H. 2019 A data-driven analysis of flash flood hazard, fatalities, and damages over the CONUS during 1996–2017. *J. Hydrol. (Amst)* **578**, 124106. https://doi.org/10.1016/j.jhydrol.2019.124106.

Alipour, A., Ahmadalipour, A. & Moradkhani, H. 2020 Assessing flash flood hazard and damages in the southeast United States. *J. Flood Risk Manage.* **13**. https://doi.org/10.1111/jfr3.12605.

Barredo, J. I. 2007 Major flood disasters in Europe: 1950–2005. *Nat. Hazard.* **42**, 125–148. https://doi.org/10.1007/s11069-006-9065-2.

Borga, M., Anagnostou, E. N., Blöschl, G. & Creutin, J. D. 2010 Flash floods: Observations and analysis of hydro-meteorological controls. *J. Hydrol. (Amst)* **394**, 1–3. https://doi.org/10.1016/j.jhydrol.2010.07.048.

Borga, M., Stoffel, M., Marchi, L., Marra, F. & Jakob, M. 2014 Hydrogeomorphic response to extreme rainfall in headwater systems: Flash floods and debris flows. *J. Hydrol. (Amst)* **518**, 194–205. https://doi.org/10.1016/j.jhydrol.2014.05.022.

Borga, M., Comiti, F., Ruin, I. & Marra, F. 2019 Forensic analysis of flash flood response. *Wiley Interdiscip. Rev. Water* **6**, 1–9. https://doi.org/10.1002/wat2.1338.

Borjalilu, N. & Bozorgi-Amiri, A. 2022 Entropy-based model for aerodromes safety risk assessment to implement safety management systems. *J. Airline Oper. Aviat. Manage.* **1**, 26–42. https://doi.org/10.56801/jaoam.v1i2.2.

Braud, I., Ayral, P. A., Bouvier, C., Branger, F., Delrieu, G., Le Coz, J., Nord, G., Vandervaere, J. P., Anquetin, S., Adamovic, M., Andrieu, J., Batiot, C., Boudevillain, B., Brunet, P., Carreau, J., Confoland, A., Didon-Lescot, J. F., Domergue, J. M., Douvinet, J., Dramais, G., Freydier, R., Gérard, S., Huza, J., Leblois, E., Le Bourgeois, O., Le Boursicaud, R., Marchand, P., Martin, P., Nottale, L., Patris, N., Renard, B., Seidel, J. L., Taupin, J. D., Vannier, O., Vincendon, B. & Wijbrans, A. 2014 Multi-scale hydrometeorological observation and modelling for flash flood understanding. *Hydrol. Earth Syst. Sci.* **18**, 3733–3761. https://doi.org/10.5194/hess-18-3733-2014.

Chen, N., Zhang, Y., Wu, J., Dong, W., Zou, Y. & Xu, X. 2020 The trend in the risk of flash flood hazards with regional development in the Guanshan River Basin, China. *Water (Switzerland)* **12**. https://doi.org/10.3390/w12061815.

Crow, W. T., Chen, F., Reichle, R. H. & Liu, Q. 2017 L band microwave remote sensing and land data assimilation improve the representation of prestorm soil moisture conditions for hydrologic forecasting. *Geophys. Res. Lett.* **44**, 5495–5503. https://doi.org/10.1002/2017GL073642.

Dinh, H. P., Vo, P. H., Pham, D. N. & Ngo, T. Q. 2022 Factors affecting farmers' decisions to participate in agricultural tourism activities: A case study in the Mekong Delta, Vietnam. *AgBioForum* **21** (3), 15–22.

Emmanuel, I., Andrieu, H., Leblois, E., Janey, N. & Janey, N. 2015 Influence of rainfall spatial variability on rainfall–runoff modelling: Benefit of a simulation approach? **531**, 337–348. https://doi.org/10.1016/j.jhydrol.2015.04.058.

Fayaz, S. A., Zaman, M. & Butt, M. A. 2022 Numerical and experimental investigation of meteorological data using adaptive linear m5 model tree for the prediction of rainfall. *Rev. Comput. Eng. Res.* **9**, 1–12. https://doi.org/10.18488/76.v9i1.2961.

Gaume, E., Bain, V., Bernardara, P., Newinger, O., Barbuc, M., Bateman, A., Blaškovičová, L., Blöschl, G., Borga, M., Dumitrescu, A., Daliakopoulos, I., Garcia, J., Irimescu, A., Kohnova, S., Koutroulis, A., Marchi, L., Matreata, S., Medina, V., Preciso, E., Sempere-Torres, D., Stancalie, G., Szolgay, J., Tsanis, I., Velasco, D. & Viglione, A. 2009 A compilation of data on European flash floods. *J. Hydrol. (Amst)* **367**, 70–78. https://doi.org/10.1016/j.jhydrol.2008.12.028.

Grillakis, M., Koutroulis, A., Komma, J., Tsanis, I., Wagner, W. & Blöschl, G. 2016 Initial soil moisture effects on flash flood generation – A comparison between basins of contrasting hydro-climatic conditions. *J. Hydrol. (Amst)* **541**, 206–217. https://doi.org/10.1016/j.jhydrol.2016.03.007.

Gu, H. & Lei, Y. 2023 Experimental investigation of the effects of the turbulence on the impact force of flash flood. *Front. Earth Sci. (Lausanne)* **10**. https://doi.org/10.3389/feart.2022.1053461.

Gultepe, I. 2023 A review on weather impact on aviation operations: Visibility, wind, precipitation, icing. *J. Airline Oper. Aviat. Manage.* **2**, 1–44. https://doi.org/10.56801/jaoam.v2i1.1.

He, B., Huang, X., Ma, M., Chang, Q., Tu, Y., Li, Q., Zhang, K. & Hong, Y. 2018 Analysis of flash flood disaster characteristics in China from 2011 to 2015. *Nat. Hazard.* **90**, 407–420. https://doi.org/10.1007/s11069-017-3052-7.

Hou, J., Guo, K., Liu, F., Han, H., Liang, Q., Tong, Y. & Li, P. 2018 Assessing slope forest effect on flood process caused by a short-duration storm in a small catchment. *Water (Switzerland)* **10**. https://doi.org/10.3390/W10091256.

Hou, J., Li, B., Tong, Y., Ma, L., Ball, J., Luo, H., Liang, Q. & Xia, J. 2020 Cause analysis for a new type of devastating flash flood. *Hydrol. Res.* **51**, 1–16. https://doi.org/10.2166/nh.2019.091.

Hou, J., Zhang, Z., Zhang, D., Shi, B, Chen, G. & Zhang, H. 2021 Study on the influence of infiltration on flood propagation with different peak shape coefficients and duration. *Water Policy* **23**, 1059–1074. https://doi.org/10.2166/wp.2021.193.

Hu, X. & Song, L. 2018 Hydrodynamic modeling of flash flood in mountain watersheds based on high-performance GPU computing. *Nat. Hazard.* **91**, 567–586. https://doi.org/10.1007/s11069-017-3141-7.

Huang, K., Chen, L., Zhou, J., Zhang, J. & Singh, V. 2018 Flood hydrograph coincidence analysis for mainstream and its tributaries. *J. Hydrol. (Amst)* **565**, 341–353. https://doi.org/10.1016/j.jhydrol.2018.08.007.

Li, J., Deng, C., Li, H., Ma, M. & Li, Y. 2018 Hydrological environmental responses of LID and approach for rainfall pattern selection in precipitation data-lacked region. *Water Resour. Manage.* **32**, 3271–3284. https://doi.org/10.1007/s11269-018-1990-9.

Liu, F., Hou, J., Guo, K., Li, D., Xu, S. & Zhang, X. 2018a High-performance numerical model for rainfall catchment process based on hydrodynamic method. *Shuidonglixue Yanjiu yu Jinzhan/Chin. J. Hydrodyn. Ser. A* **33**, 778–785. https://doi.org/10.16076/j.cnki.cjhd.2018.06.015.

Liu, Y., Yang, Z., Huang, Y. & Liu, C. 2018b Spatiotemporal evolution and driving factors of China's flash flood disasters since 1949. *Sci. China Earth Sci.* **61**, 1804–1817. https://doi.org/10.1007/s11430-017-9238-7.

Llasat, M., Marcos, R., Llasat-Botija, M., Gilabert, J., Turco, M. & Quintana-Seguí, P. 2014 Flash flood evolution in North-Western Mediterranean. *Atmos. Res.* **149**, 230–243. https://doi.org/10.1016/j.atmosres.2014.05.024.

Lobligeois, F., Andréassian, V., Perrin, C., Tabary, P. & Loumagne, C. 2014 When does higher spatial resolution rainfall information improve streamflow simulation? An evaluation using 3620 flood events. *Hydrol. Earth Syst. Sci.* **18**, 575–594. https://doi.org/10.5194/hess-18-575-2014.

Marchi, L., Borga, M., Preciso, E. & Gaume, E. 2010 Characterisation of selected extreme flash floods in Europe and implications for flood risk management. *J. Hydrol. (Amst)* **394**, 118–133. https://doi.org/10.1016/j.jhydrol.2010.07.017.

Ming, X., Liang, Q. & Xia, X. 2020 Real-time flood forecasting based on a high-performance 2-D hydrodynamic model and numerical weather predictions. *Water Resour. Res.* **56**. https://doi.org/10.1029/2019WR025583.

Novák, P., Kyznarová, H., Pecha, M., Šercl, P., Svoboda, V. & Ledvinka, O. 2021 Utilization of weather radar data for the flash flood indicator application in the Czech Republic. *Remote Sens. (Basel)* **13**. https://doi.org/10.3390/rs13163184.

Oborie, E. & Rowland, E. D. 2023 Flood influence using GIS and remote sensing based morphometric parameters: A case study in Niger delta region. *J. Asian Sci. Res.* **13**, 1–15. https://doi.org/10.55493/5003.v13i1.4719.

Ochoa-Rodriguez, S., Wang, L., Gires, A., Daniel, R., Reinoso-rondinel, R., Bruni, G., Ichiba, A., Gaitan, S., Cristiano, E., Assel, J., Kroll, S., Murlà-tuyls, D., Tisserand, B., Schertzer, D., Tchiguirinskaia, I., Onof, C., Willems, P. & Veldhuis, M. 2015 Impact of spatial and temporal resolution of rainfall inputs on urban hydrodynamic modelling outputs: A multi-catchment investigation. *J. Hydrol. (Amst)* **531**, 389–407. https://doi.org/10.1016/j.jhydrol.2015.05.035.

Peleg, N., Blumensaat, F., Molnar, P., Fatichi, S. & Burlando, P. 2017 Partitioning the impacts of spatial and climatological rainfall variability in urban drainage modeling. *Hydrol. Earth Syst. Sci.* **21**, 1559–1572. https://doi.org/10.5194/hess-21-1559-2017.

Rogger, M., Agnoletti, M., Alaoui, A., Bathurst, J., Bodner, G., Borga, M., Chaplot, V., Gallart, F., Glatzel, G., Hall, J., Holden, J., Holko, L., Horn, R., Kiss, A., Quinton, J., Leitinger, G., Lennartz, B., Parajka, J., Peth, S., Robinson, M., Salinas, J., Santoro, A., Szolgay, J., Tron, S. & Viglione, A. 2017 Land use change impacts on floods at the catchment scale: Challenges and opportunities for future research. *Water Resour. Res.* **53**, 5209–5219. https://doi.org/10.1002/2017WR020723.

Saharia, M., Kirstetter, P. & Vergara, H. 2021 On the impact of rainfall spatial variability, geomorphology, and climatology on flash floods. *Water Resour. Res.* 1–18. https://doi.org/10.1029/2020WR029124.

Samadi, M., Sarkardeh, H. & Jabbari, E. 2020 Explicit data-driven models for prediction of pressure fluctuations occur during turbulent flows on sloping channels. *Stochastic Environ. Res. Risk Assess.* **34**, 691–707. https://doi.org/10.1007/s00477-020-01794-0.

Samadi, M., Sarkardeh, H. & Jabbari, E. 2021 Prediction of the dynamic pressure distribution in hydraulic structures using soft computing methods. *Soft Comput.* **25**, 3873–3888. https://doi.org/10.1007/s00500-020-05413-6.

Silvestro, F., Rebora, N., Giannoni, F., Cavallo, A. & Ferraris, L. 2016 The flash flood of the Bisagno Creek on 9th October 2014: An 'unfortunate' combination of spatial and temporal scales. *J. Hydrol. (Amst)* **541**, 50–62. https://doi.org/10.1016/j.jhydrol.2015.08.004.

Simons, F., Busse, T., Hou, J., Özgen, I. & Hinkelmann, R. 2014 A model for overland flow and associated processes within the Hydroinformatics Modelling System. *J. Hydroinf.* **16**, 375–391. https://doi.org/10.2166/hydro.2013.173.

Wang, W. & Wang, Y. 2022 Research on image capture technology of intelligent terminal and multi exposure fusion to improve the resilience of agriculture production systems. *J. Commer. Biotechnol.* **27**, 46–56. https://doi.org/10.5912/jcb1045.

Wei, Z., Sun, H., Xu, H., Wu, G. & Xie, W. 2019 The effects of rainfall regimes and rainfall characteristics on peak discharge in a small debris flow-prone catchment. *J. Mt Sci.* **16**, 1646–1660. https://doi.org/10.1007/s11629-018-5260-3.

Wright, D. B. 2018 Rainfall information for global flood modeling. In Geophysical Monograph Series (Schumann, G. J.-P., Bates, P. D., Apel, H. & Aronica, G. T., eds.). Wiley, Hoboken, NJ, pp. 17–42.

Wright, D. B., Smith, J. A. & Baeck, M. L. 2014 Flood frequency analysis using radar rainfall fields and stochastic storm transposition. *Water Resour. Res.* **50**, 1592–1615. https://doi.org/10.1002/2013WR014224.

Wright, D. B., Yu, G. & England, J. F. 2020 Six decades of rainfall and flood frequency analysis using stochastic storm transposition: Review, progress, and prospects. *J. Hydrol. (Amst)* **585**, 124816. https://doi.org/10.1016/j.jhydrol.2020.124816.

Yang, L., Smit, J. A., Baeck, M. L. & Zhang, Y. 2016 Flash flooding in small urban watersheds: Storm event hydrologic response. *Water Resour. Res.* **52**, 4571–4589. https://doi.org/10.1002/2015WR018326.

Zhou, Z., Smith, J. A., Baeck, M. L., Wright, D. B., Smith, B. K. & Liu, S. 2021 The impact of the spatiotemporal structure of rainfall on flood frequency over a small urban watershed: An approach coupling stochastic storm transposition and hydrologic modeling. *Hydrology and Earth System Sciences* **25** (9), 4701–4717.

Zhu, Z., Wright, D. B. & Yu, G. 2018 The impact of rainfall space-time structure in flood frequency analysis. *Water Resour. Res.* **54**, 8983–8998. https://doi.org/10.1029/2018WR023550.

Zwawi, M. & Algarni, M. 2019 Optimal stormwater runoff path by identifying gravitational potential energy function with the least energy path. *J. Manage. Eng. Integr.* **12**, 78–85.

First received 13 September 2023; accepted in revised form 12 December 2023. Available online 26 December 2023